Available online at www.sciencedirect.com
SCIENCE DIRECT®
Journal of Power Sources 140 (2005) 350–354
JOURNAL OF POWER SOURCES
www.elsevier.com/locate/jpowsour

Solvothermal synthesis and electrochemical performances of nanosized $CoSb_3$ as anode materials for Li-ion batteries

J. Xie, X.B. Zhao*, G.S. Cao, M.J. Zhao, S.F. Su

Department of Materials Science and Engineering, Zhejiang University, Hangzhou 310027, PR China

Received 19 May 2004; received in revised form 5 July 2004; accepted 23 August 2004

Abstract

In the present study, the $CoSb_3$ powder was prepared by solvothermal route for the first time and the particle size of the as-prepared powder is in nanoscale. The electrochemical performances of the nanosized $CoSb_3$ were characterized by galvanostatic charge and discharge cycling, cyclic voltammogram (CV) and electrochemical impedance spectroscopy (EIS). The electrochemical lithiation and delithiation mechanism of $CoSb_3$ compound was investigated by ex situ XRD (X-ray diffraction) technique. The large reversible capacity and good cycling stability of nanosized $CoSb_3$ suggest that it stands as a promising anode material for secondary Li-ion batteries.

Keywords: $CoSb_3$; Anode material; Solvothermal synthesis; Nanosized materials; Li-ion batteries

1. Introduction

Lithium-ion batteries are state-of-the-art power sources for portable electronic devices such as camcorders, mobile telephones and laptop computers, due to their high working voltage and energy density. Carbon-based materials are currently used as anode materials due to the flat charge and discharge plateau and excellent cycling stability. However, their theoretical maximum capacity is limited to 372 mAh g^{-1} corresponding to the formation of LiC_6 stoichiometry [1]. Since the introduction of tin-based oxide composite by Fuji Photo Film Celltec in early 1997 [2], great interest has been turned to metal or alloy anodes due to their extremely larger capacity compared to those of carbon-based materials.

Among these alloys, which can be potential anode materials for secondary Li-ion batteries, the Sb-based intermetallic compounds received much interest in recent years. Alcántara et al. [3] first reported $CoSb_3$ as the anode materials for Li-ion batteries. After that, a number of Sb-based intermetallic compounds, such as $CrSb_2$ [4], $TiSb_2$ [5], Cu_2Sb [6], Mn_2Sb [7], $Co_{1-2y}Fe_yNi_ySb_3$ [8], SnSb [9], etc., are intensively investigated. Although these compounds show slight lower capacity than pure Sb (660 mAh g^{-1}), they exhibit improved cycling behavior. Unfortunately, the long-term cycleability cannot meet the requirement for the practical application of these compounds as anode in commercial Li-ion batteries. The main drawback of these compounds is the rapid capacity fade upon repeated cycling resulting from the large volume changes during the charge and discharge cycling.

The use of thin-film materials seems to be an effective strategy to alleviate the volume change effect since the thin-film materials have higher surface/thickness ratio than bulk materials. Recent studies of electrochemical performances on thin-film Co–Si [10], Ag [11], SiAlSn [12], Ni_3Sn_2 [13] and NiO [14] anodes show that thin-film materials have a potential application in Li-ion batteries, especially for microelectronic devices. More recently, the electrochemical properties of thin-film $CoSb_3$ have also been investigated by Pralong et al. [15]. The use of nanosized materials seems another strategy to mitigate the volume change effect of the intermetallic electrodes due to the small particle size and large specific surface area of nanosized materials, thus lessens

* Corresponding author. Tel.: +86 571 8795 1451; fax: +86 571 8795 1403.
E-mail address: zhaoxb@zju.edu.cn (X.B. Zhao).

0378-7753/$ – see front matter © 2004 Elsevier B.V. All rights reserved.
doi:10.1016/j.jpowsour.2004.08.027

the absolute volume changes. In our present work, nanosized $CoSb_3$ powder was synthesized by solvothermal route. The electrochemical performances of this material were investigated by galvanostatic cycling, cyclic voltammogram (CV) and electrochemical impedance spectroscopy (EIS). Ex situ XRD technique was also used to study the electrochemical lithiation and delithiation mechanism of $CoSb_3$ compound.

2. Experimental

The nanosized $CoSb_3$ was prepared by solvothermal route. $CoCl_2{\cdot}6H_2O$ (10 mmol), $SbCl_3$ (30 mmol) and $NaBH_4$ (110 mmol) were put into a Teflon-lined autoclave that had been filled with anhydrous ethanol up to 85% of its 160 ml capacity. The autoclave was maintained at 190 °C for 24 h, then the temperature was elevated to 240 °C and maintained it for 48 h, and then cooled to room temperature naturally. The precipitate was filtered, washed with anhydrous ethanol and distilled water in sequence, and then dried at 110 °C under vacuum for 12 h.

The phases present in the alloy powder were identified by powder X-ray diffraction (XRD) using a Rigaku-D/MAX-2550PC diffractometer equipped with Cu K_α radiation ($\lambda = 1.5406$ Å) in the 2θ range of 10–80° with steps of 0.02°. The morphology of the $CoSb_3$ powder was observed by transmission electron microscopy (TEM) on a JEM-2110 TEM.

The electrochemical reactions of $CoSb_3$ alloy with lithium were investigated using a simple two-electrode cell: Li/$LiPF_6$ (EC + DMC)/$CoSb_3$. The working electrode consists of 80 wt.% $CoSb_3$ powder, 10 wt.% acetylene black as conducting agent and 10 wt.% PVDF (polyvinylidene fluoride) as binder. The cells were assembled in an Ar-filled glove box using PP (polypropylene) micro-porous film as separator, a solution of 1 M $LiPF_6$ in EC (ethylene carbonate)/DMC (dimethyl carbonate) (1:1 in volume) as electrolyte and metallic lithium foil as counter electrode. The cells are galvanostatically charged/discharged at a current density of 20 mA g^{-1} between 0.05 and 1.5 V versus Li^+/Li. The CV test was performed with a scanning rate of 0.1 mV s^{-1} between 0.05 and 2 V on an Arbin-001 MITS 2.9-BT2000 instrument. EIS measurements were carried out using a Solartron FRA 1250 frequency responses analyzer combined with a Solartron SI 1287 electrochemical interface. The impedance spectra were recorded potentiostatically by applying an ac voltage of 5 mV amplitude over the frequency range from 1 MHz to 0.1 Hz after the cells were left at the delithiated state for 24 h to achieve equilibrium.

Ex situ XRD was performed to investigate the electrochemical lithiation and delithiation mechanism of $CoSb_3$. The XRD patterns were collected on the $CoSb_3$ electrodes at desired charged states during the first cycle. The model cells were dismantled in the Ar-filled glove box and the electrodes were covered with PE (polyethylene) film in order to minimize the air exposure and were then transferred to the XRD analysis chamber. XRD data of $CoSb_3$ were collected in the 2θ range of 10°–80° with steps of 0.02°.

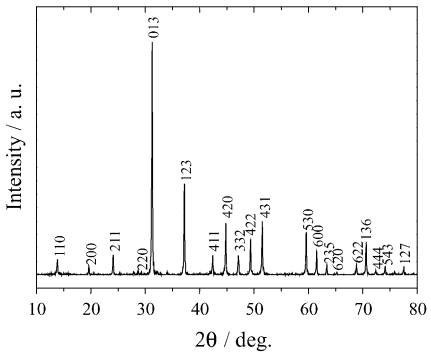

Fig. 1. XRD patterns of $CoSb_3$ powder prepared by solvothermal route.

3. Results and discussion

Fig. 1 shows the XRD patterns of $CoSb_3$ powder prepared by solvothermal route. The diffraction peaks can be indexed as skutterudite-type $CoSb_3$ phase with space group *Im*3 [16]. The lattice parameter calculated from the diffraction data is $a = 9.033$ Å, which is in good agreement with the literature value ($a = 9.034$ Å) [16]. According to XRD results, the synthesis reactions can be written as:

$$CoCl_2 + 2NaBH_4 \rightarrow Co + 2BH_3 + H_2 + 2NaCl \quad (1)$$

$$SbCl_3 + 3NaBH_4 \rightarrow Sb + 3BH_3 + \tfrac{3}{2}H_2 + 3NaCl \quad (2)$$

$$Co + 3Sb \rightarrow CoSb_3 \quad (3)$$

Fig. 2 shows the TEM images of $CoSb_3$ powder prepared by solvothermal route. Note that the $CoSb_3$ particles are composed of small granules with particle size below 20 nm and large aggregates with size above 60 nm. The shapes of both small granules and large aggregates are irregular. It seems that the particles are connected each other and form a network structure. As a result, the particle size of $CoSb_3$ powder prepared by solvothermal route is in nanoscale.

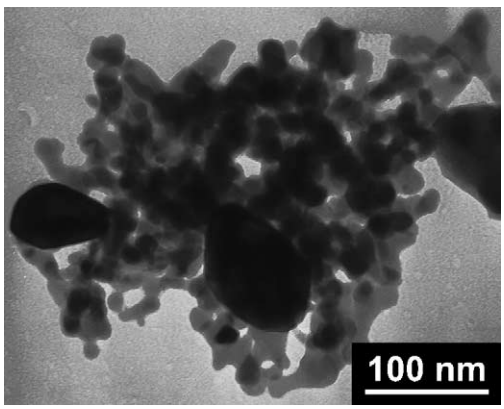

Fig. 2. TEM images of $CoSb_3$ powder prepared by solvothermal synthesis.

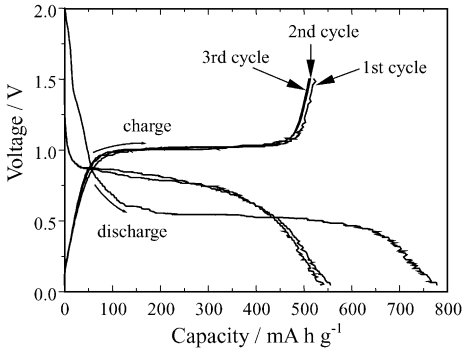

Fig. 3. Charge and discharge curves of nanometric $CoSb_3$ electrode for the first three cycles.

Fig. 3 shows the charge and discharge curves of nanometric $CoSb_3$ electrode. It is clear that apart from the first discharge process, the nanometric $CoSb_3$ electrode exhibits a high reversibility evidenced by the almost overlapped charge or discharge curves. The first reversible capacity of nanometric $CoSb_3$ electrode reaches 521 mAh g^{-1}, which is close to its theoretical capacity of 568 mAh g^{-1}, corresponding to the formation of Li_3Sb composition. Considering the high density (7.25 g cm^{-3}) of $CoSb_3$ compound, the volumetric capacity of $CoSb_3$ reaches 3770 mAh cm^{-3}, which is over four times higher than that of carbon-based materials (800 mAh cm^{-3}). As a result, the nanometric $CoSb_3$ arises as a high-capacity anode material for secondary Li-ions batteries.

Fig. 4 compares the cycling behavior between nanometric and micrometric $CoSb_3$ electrodes. Only slight capacity fade is observed for the nanometric $CoSb_3$ electrode for the 10 cycles. The good cycling behavior is related to the microstructure of nanometric $CoSb_3$. The reduced particle size for nanometric $CoSb_3$ decreases the Li-ions diffusion path and thus causes the small absolute volume change. In addition, the large specific surface area of nanometric $CoSb_3$ maximizes the contacts between active material and electrolyte solution, thus improving kinetics for the lithiation and delithiation reactions. Consequently, the cycling stability is enhanced. Note that the electrochemical performances of nanometric $CoSb_3$ electrode are greatly improved compared to that of the micrometric counterpart as shown clearly in the figure. The poor cycling behavior for micrometric $CoSb_3$ is related to its large absolute volume change upon cycling and sluggish Li-ions diffusion kinetics. Note that the first irreversible capacity (defined as the difference between the first lithiation capacity and first delithiation capacity) for micrometric $CoSb_3$ (311 mAh g^{-1}) is larger for nanometric one (257 mAh g^{-1}). This is due to the fact that the micrometric sample is prepared by ball milling, and ball milling often introduces impurities and defects facilitating the decomposition reactions of electrolyte solution and formation of the SEI layer.

Fig. 5 shows the cyclic voltammogram (CV) curves of the nanometric $CoSb_3$ electrode for the first three cycles. Apart from the first cycle, the electrode exhibits high reversibility as can seen from the almost overlapped CV curves, which is in good agreement with the enhanced electrochemical performances of the nanometric $CoSb_3$ electrode. The cathodic anodic and peaks, which are positioned at around 0.6 and 1.2 V, respectively, correspond to the lithiation and delithiation plateaus in the charge and discharges curves. However, the cathodic peak for the first cycle is not well developed, which may be ascribed to the sluggish kinetics of first lithiation process which can be described as a process of the decomposition of $CoSb_3$ structure and the accompanied structural reconstruction within the electrode system.

Ex situ XRD was used to investigate the lithiation and delithiation mechanism of the nanometric $CoSb_3$ in our present work. The XRD patterns at desired charged state are summarized in Fig. 6. No obvious changes in the XRD patterns can be observed when the electrode is discharged to 0.6 V, which means the basic $CoSb_3$ structure is maintained above such a potential. The lithiation capacity above this potential is attributed to the decomposition of the electrolyte solution and the subsequent formation of solid electrolyte interface (SEI) layer [17] composing mainly of Li_2CO_3 and $(CH_2OCO_2Li)_2$ which irreversibly consume some Li-ions and account for the large first discharge capacity (about 750 mAh g^{-1}). When the electrode is polarized to 0.05 V, the

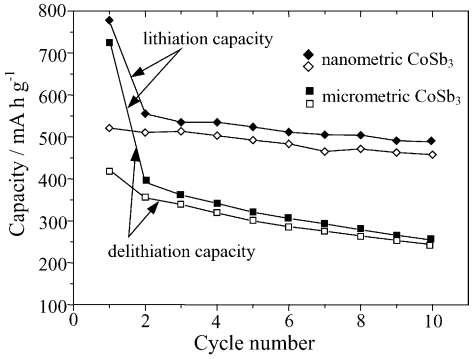

Fig. 4. Comparison of cycling behavior between nanometric and micrometric $CoSb_3$ electrodes.

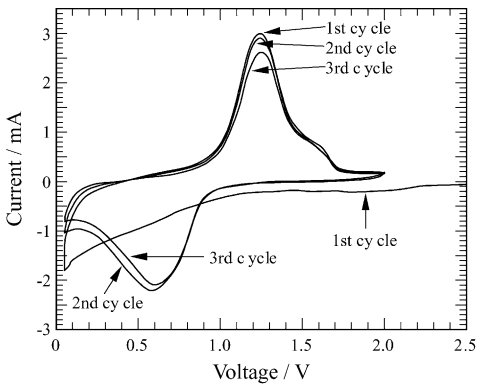

Fig. 5. cyclic voltammogram of nanometric $CoSb_3$ electrode for the first three cycles. The scanning rate is 0.1 mV s^{-1}.

Table 1
Fitting results of Nyquist plots using the equivalent circuit

Sample	R_s (Ω)	R_1 (Ω)	R_2 (Ω)	R_w (Ω)
As-prepared	5.16 ± 0.02	234.7 ± 2.3	31.7 ± 1.4	893.2 ± 27.7
Discharged to 0.94 V	6.98 ± 0.05	112.0 ± 1.5	0.97 ± 0.46	56.9 ± 6.6
Discharged to 0.4 V	5.05 ± 0.96	63.0 ± 1.4	2.13 ± 0.73	83.7 ± 6.1
Charged to 0.96 V	9.58 ± 0.15	40.3 ± 1.9	6.4 ± 1.3	66.9 ± 6.9
Charged to 1.48 V	8.23 ± 0.18	49.3 ± 4.3	5.8 ± 2.8	377.4 ± 9.2

$CoSb_3$ peaks are significantly reduced and broadened with the appearance of Li_3Sb peaks. So, the first discharge process can be written as:

$$CoSb_3 + 9Li^+ + 9e^- \rightarrow 3Li_3Sb + Co \quad (4)$$

Li_3Sb peaks, however, are not well resolved under present condition due to the complicated electrode system and the large background peaks. Note that the $CoSb_3$ structure is not recovered even though at full delithiated state (charged to 1.5 V). This means the $CoSb_3$ structure undergoes irreversible decomposition upon first discharge process. According to the ex situ XRD and the CV results, the chare and discharge reactions during the subsequent cycling can be written as:

$$Li_3Sb \leftrightarrow Sb\,3Li^+ + 3e^-$$

Under such a condition, Li_3Sb or Sb, rather than $CoSb_3$, can be considered as the true rechargeable anode. It should be mentioned that the cobalt diffraction peaks are absent in the XRD patterns. In our opinion, the cobalt may be in the amorphous state or in nanoscale.

To further study the lithiation and delithiation mechanism of nanometric $CoSb_3$ electrode, EIS was carried out. The spectra evolution at the desired voltages are summarized in Fig. 7(a). The impedance spectra are fitted with the equivalent circuit as seen in Fig. 7 (b). According to the literature [18], R_s represents the solution resistance, R_1 and CPE_1 signify the diffusion resistance of Li-ions through the solid electrolyte interface (SEI) layer and the corresponding constant phase element (CPE), R_2 and CPE_2 correspond to the charge transfer resistance and the corresponding the CPE, while R_w is related to the solid state diffusion of Li-ions in the active materials corresponding to the slopping line at the low frequency. The fitting results of Nyquist plots by equivalent circuit (shown in Table 1) indicate that the as-prepared nanometric $CoSb_3$ electrode exhibits extremely large R_1 value which decreases rapidly on first discharge. Generally speaking, the as-prepared electrode should not show such a large SEI resistance. In our opinion, the large R_1 comes mainly from Li counter electrode with small contribution from SEI resistance even the precise separation of the two kinds of resistances is difficult due to the complicated electrode system. The large change of resistance means that the nanometric $CoSb_3$ electrode undergoes a great structural reconstruction in the first discharge process, during which, the electrode is activated with the reduced electrode resistance, and the Li surface area may be on the increase evidenced by the rapid reduced R_1 value. Notice that the resistance changes during the charge process are smaller than that during the discharge process indicating less drastic microstructure changes.

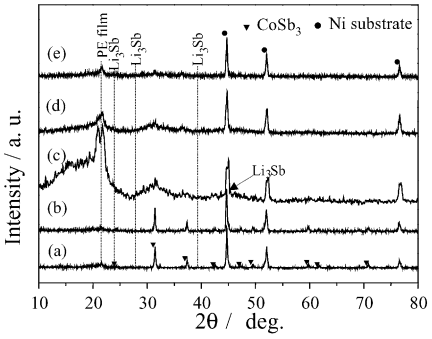

Fig. 6. Ex situ XRD patterns of nanometric $CoSb_3$ electrodes for fresh electrode (a), discharged to 0.6 V (b), discharged to 0.05 V (c), charged to 1.0 V (d), and charged to 1.5 V (e).

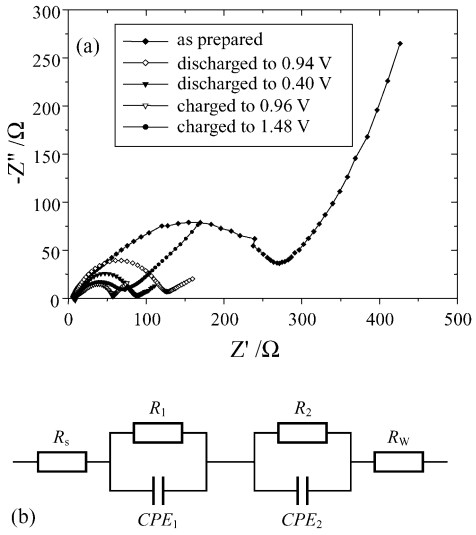

Fig. 7. EIS plots of nanometric $CoSb_3$ electrodes at different voltages (a) and the corresponding equivalent circuit (b).

4. Conclusions

In this paper, nanosized $CoSb_3$ was prepared by solvothermal method, and its electrochemical lithiation and delithiation performances were investigated by several electroanalytical techniques, namely, galvanostatic cycling, CV and EIS. The nanoscaled $CoSb_3$ exhibits improved capacity retention

compared to its micrometric counterpart due to the nanodispersion effect.

Acknowledgements

The work is supported by National Natural Science Foundation of China (50201014), the “863” Program of China (2002AA323060) and by PFDP of the Education Ministry of China (20010335045).

References

[1] R. Fong, U.V. Sacken, J. Electrochem. Soc. 137 (1990) 2009.
[2] Y. Idota, T. Kubata, A. Matsufuji, Y. Maekawa, T. Miyasaka, Science 276 (1997) 1395.
[3] R. Alcántara, F.J. Fernández-Madrigal, P. Lavela, J.L. Tirado, J.C. Jumas, J. Olivier-Fourcade, J. Mater. Chem. 9 (1999) 2517.
[4] F.J. Fernández-Madrigal, P. Lavela, C. Pérez-Vicente, J.L. Tirado, J. Electroanal. Chem. 501 (2001) 205.
[5] D. Larcher, L.Y. Beaulieu, O. Mao, A.E. George, J.R. Dahn, J. Electrochem. Soc. 147 (2000) 1703.
[6] L.M.L. Fransson, J.T. Vaughey, R. Benedek, K. Edström, J.O. Thomas, M.M. Thackeray, Electrochem. Commun. 3 (2001) 317.
[7] L.M.L. Fransson, J.T. Vaughey, K. Edström, M.M. Thackeray, J. Electrochem. Soc. 150 (2003) 86.
[8] L. Monconduit, J.C. Jumas, R. Alcántara, J.L. Tirado, C. Pérez Vicente, J. Power Sources 107 (2002) 74.
[9] J.O. Besenhard, M. Wachtler, M. Winter, R. Andreus, I. Rom, W. Sitte, J. Power Sources 81–82 (1999) 268.
[10] Y.L. Kim, H.Y. Lee, S.W. Jang, S.H. Lim, S.J. Lee, H.K. Baik, Y.S. Yoon, S.M. Lee, Electrochim. Acta 48 (2003) 593.
[11] G. Taillades, J. Sarradin, J. Power Sources 125 (2004) 199.
[12] T.D. Hatchard, J.M. Topple, M.D. Fleischauer, J.R. Dahn, Electrochem. Solid-State Lett. 6 (2003) 129.
[13] Y.L. Kim, H.Y. Lee, S.W. Jang, S.J. Lee, H.K. Baik, Y.S. Yoon, Y.S. Park, S.M. Lee, Solid State Ionics 160 (2003) 235.
[14] Y. Wang, Y.F. Zhang, H.R. Liu, S.J. Yu, Q.Z. Qin, Electrochim. Acta 48 (2003) 4253.
[15] V. Pralong, J.B. Leriche, B. Beaudoin, E. Naudin, M. Morcrette, J.M. Tarascon, Solid State Ionics 166 (2004) 295.
[16] JCPDS card No. 76-0470.
[17] D. Aurbch, Y. Ein-Eli, B. Markovsky, A. Zaban, J. Electrochem. Soc. 142 (1995) 2882.
[18] Y.C. Chang, J.H. Jong, G.T.K. Fey, J. Electrochem. Soc. 147 (2000) 2033.